# Nanoscale

Accepted Manuscript


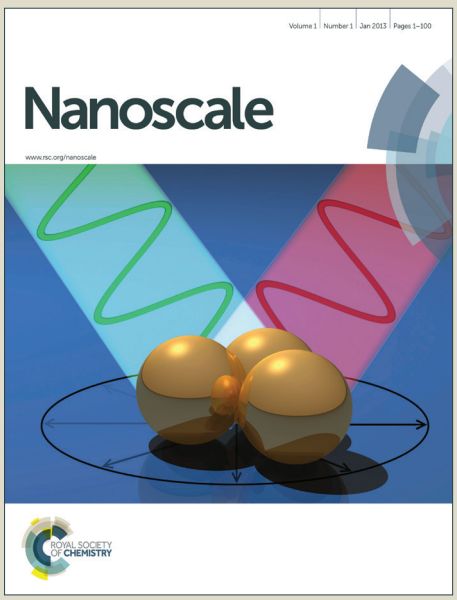





ROYAL SOCIETY OF CHEMISTRY

www.rsc.org/nanoscale

Nanoscale

COMMUNICATION

# Real-time monitoring of oxidative etching on single Ag nanocube via light-scattering dark-field microscopic imaging

Received 00th January 20xx,
Accepted 00th January 20xx

DOI: 10.1039/x0xx00000x

www.rsc.org/

Yi Wang,[a,b] Hong Yan Zou[a] and Cheng Zhi Huang[a,*]

**A low-cost and easy-conducted light-scattering dark-field microscopic imaging (iDFM) technique for real-time and in situ monitoring of the oxidative etching occurred on a single Ag nanocube was presented by using an ordinary dark-field microscopic system, which provides an alternative approach to study the behaviors of metal nanoparticles in chemical reactions and biological processes at single nanoparticle level.**

Metal nanoparticles (NPs) with different shapes and architectures have received considerable attention in recent years due to their remarkable physicochemical properties and performances in optics, electronics, catalysis, and biomedicine.[1] Thus, understanding the mechanisms responsible for NP nucleation, growth, self-assembly, and etching has become a hot topic of intense study in order to achieve novel structures and shape-dependent properties. For this purpose, a variety of different techniques have been developed to monitor the behaviors of metal NPs, including small-angle X-ray scattering (SAXS),[2] optical spectroscopy,[3] time-resolved X-ray diffraction (XRD),[4] atomic force microscopy (AFM),[5] and liquid cell transmission electron microscopy (TEM).[6] However, these approaches are still limited by their intrinsic shortcomings. For example, optical spectroscopy and XRD can only record the collective signals of all the NPs and thus are unable to resolve the individual NPs; SAXS records data in the reciprocal space and needs complex analysis to obtain real space structural information; AFM can hardly monitor the NPs-involved reactions in a real-time mode owing to its relatively slow scanning speed.

Recently, the development of *in situ* liquid TEM provides a powerful means to directly visualize the growth and self-assembly of individual particles in nanoscale. For instance, real-time and *in situ* monitoring of the growth of Pt NPs[6a] and $Pt_3Fe$ nanorods,[6d] self-assembly of charged Au NPs,[6e] as well as the oxidative etching of Pd nanocrystals[6f] have been successfully achieved. However, the *in situ* liquid TEM is too expensive to allow the development of such technique in ordinary laboratories. To this end, it is necessary to develop an alternative method to real-time and *in situ* visualize the behaviors of metal NPs. In this paper, based on the localized surface plasmon resonance (LSPR) optical properties of metal NPs, we developed a light-scattering dark-field microscopy and thus achieved the real-time and *in situ* monitoring of oxidative etching process of metal NPs on single-particle level.

Oxidative etching is a common phenomenon in our daily life (*e.g.*, corrosion), which has been found to play an important role in the synthesis of metal nanocrystals with well-defined structures.[7] Therefore, understanding the mechanism involved in the etching process is significant for material synthesis and applications. In this regard, extensive studies on the wet etching have been carried out, and metal nanocrystals with specific crystallinities, shapes, and structures have been obtained.[8] However, the previous reports are unable to resolve the etching process on the same individual NP. Thus, the mechanism involved in the oxidative etching can only be learned from the experimental results of a batch of NPs (or combined with the simulations on single NP). Very recently, Zhang and co-workers achieved the *in situ* study of oxidative etching of individual Pd nanocrystals.[6f] However, as the same as other groups, they still needed to use a very expensive liquid cell electron microscope.

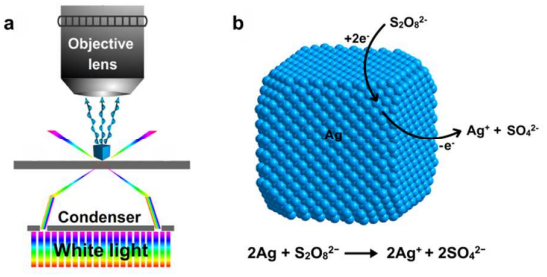


**Fig. 1** Schematic illustration showing (a) the light-scattering dark-field microscopic system used in this work and (b) the mechanism of oxidative etching of an AgNC by a specific etchant (take $S_2O_8^{2-}$ as an example).

[a] *Key Laboratory of Luminescent and Real-Time Analytical Chemistry, Ministry of Education, College of Pharmaceutical Sciences and College of Chemistry and Chemical Engineering, Southwest University, Chongqing 400715, P. R. China*
[b] *Key Laboratory of Green Synthesis and Applications, and College of Chemistry, Chongqing Normal University, Chongqing 401331, P. R. China*
*E-mail: chengzhi@swu.edu.cn; Fax: (+86)-23-68367257*
Electronic Supplementary Information (ESI) available: experimental section and additional results. See DOI: 10.1039/x0xx00000x

To overcome these shortcomings, we herein developed an alternative optical microscopy to achieve the real-time and *in situ* monitoring of oxidative etching on single-particle level. Combining the experimental results and simulation, it is demonstrated that the oxidative etching occurred on a single Ag nanocube (AgNC) is a thermodynamics-dependent process. Namely, compared with the {100} facets of a nanocube, the sharp corners can be preferentially etched and thus form a quasi-spherical particle owing to the relatively higher surface energy of the corner sites. More importantly, we have demonstrated that the present technique is a simple and universal approach to real-time and *in situ* visualization of the behaviors of metal NPs.

Fig. 1 shows the schematic illustration of the real-time and *in situ* monitoring of oxidative etching of an individual AgNC. Since the AgNPs have very large scattering cross-section, the strong LSPR scattering light of the individual particles can be easily resolved using light-scattering dark-field microscopy.[9] In the present work, the AgNCs were first deposited on the flow cell with an appropriate density. After crossing a dark-field condenser, the white light could excite the AgNCs to generate colored scattering light, which was collected by a true-color CCD camera from a 100× object lens. A common etchant, $K_2S_2O_8$, was used to interact with the AgNCs for etching. Because the standard electrode potential of $S_2O_8^{2-}/SO_4^{2-}$ (2.0 V versus RHE) is more positive than that of $Ag^+/Ag$ (0.8 V versus RHE), AgNCs can be oxidized/etched by $K_2S_2O_8$ according to the following equation:

$$2Ag_{(s)} + S_2O_8^{2-}{}_{(aq)} \rightarrow 2Ag^+_{(aq)} + 2SO_4^{2-}{}_{(aq)}$$

In this reaction, it is supposed that the Ag atoms will be oxidized to $Ag^+$ and dissolved in the solution in the presence of $S_2O_8^{2-}$. As a result, the morphology of the AgNCs will be changed. It is well known that the LSPR properties of noble metal NPs can be dramatically affected by the particle composition, shape, size, and surrounding medium.[10] Thus, the changes of the LSPR scattering signal of the AgNCs are able to be recorded for real-time monitoring of the oxidative etching process.

The AgNCs were prepared in polyols using a two-step approach.[11] Firstly, uniform Ag seeds of ~22 nm in size were synthesized in diethylene glycol, and then AgNCs with edge length of 45.2±2.3 nm were prepared by a seed-mediated growth method. Scanning electron microscopy (SEM) and TEM images show that the as-obtained AgNCs were very uniform in size, and the purity of cubic shape exceeded 95% (Fig. 2a and 2b). UV-vis spectrum shows the main LSPR peak (corresponding to the dipole resonance) of the ~45 nm AgNCs was located at 437 nm (see Fig. S1 in Supporting Information). Thus, these AgNCs scattered uniform blue-green light under a dark-field microscope, as shown in Fig. 2c and 2d. In order to obtain the quantitative information of a specific AgNC, we used the software of Image-Pro Plus to analyze the dark-field images. Fig. 2e shows the scattering light intensities of the AgNCs corresponded to the image in Fig. 2d (marked as particles 1-3). Moreover, the color of the particles could also be quantitatively recorded by splitting the color into red (R), green (G), and blue (B) with their own percentages.[12] For example, it was found that the percentage of blue (PB) and green (PG) were dominant (close to 60% and 40% for PB and PG, respectively), while less than 10% (PR) was corresponded to the red color (Fig. 2f). The quantitative data were identical with the blue-green color of the AgNCs in the images that

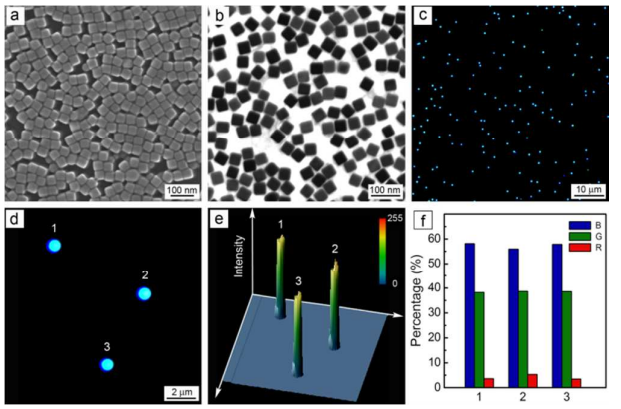


**Fig. 2** Morphology and optical properties of the AgNCs: (a) SEM image; (b) TEM image; (c) light-scattering dark-field microscopic image; (d) light-scattering dark-field image of typical individual AgNCs with higher magnification; (e) intensity analysis of the AgNCs shown in (d); (f) RGB analysis of the AgNCs shown in (d).

recorded by microscope, demonstrating that the LSPR scattering light of individual metal NPs can be quantitatively analyzed and precisely transferred to numerical information.

To directly validate the relationship between the morphology and scattering light of the same particle, we obtained the dark-field optical image and corresponding SEM image at the same region by a smart co-location technique.[9c] As shown in Fig. 3, the AgNCs (marked as No. 1-11) showed the same locations and distances between each other in both light-scattering dark-field microscopic image and SEM image, demonstrating that the observed scattering light indeed came from the corresponding individual AgNCs. This co-location technique was conducive to study the shape-dependent optical properties of individual metal nanoparticles.

Then, the real-time scattering light of individual AgNPs during the oxidative etching process was monitored with the aid of a dark-field microscope. The optical information of the individual AgNPs at different time points was also recorded and quantitatively analyzed. It was found that dynamic change of the scattering light of the AgNCs occurred after they had been exposed to 100 mM of $S_2O_8^{2-}$ (Movie S1 and Fig. S2 in Supporting Information). Specifically, the scattering light of AgNCs changed from blue-green to cyan, cyan-green, and green with increased reaction time, together with the decrease of light intensity. After 26 min, the scattering light of all

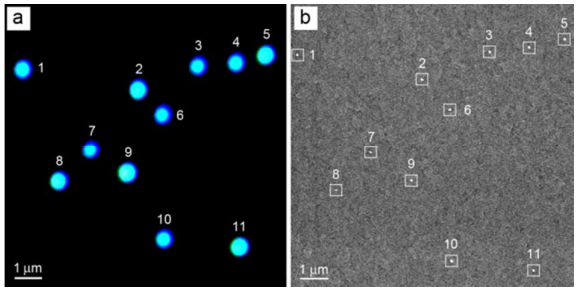


**Fig. 3** a) Light-scattering dark-field microscopic image and b) SEM images of the AgNCs located at the same area.

Nanoscale

COMMUNICATION

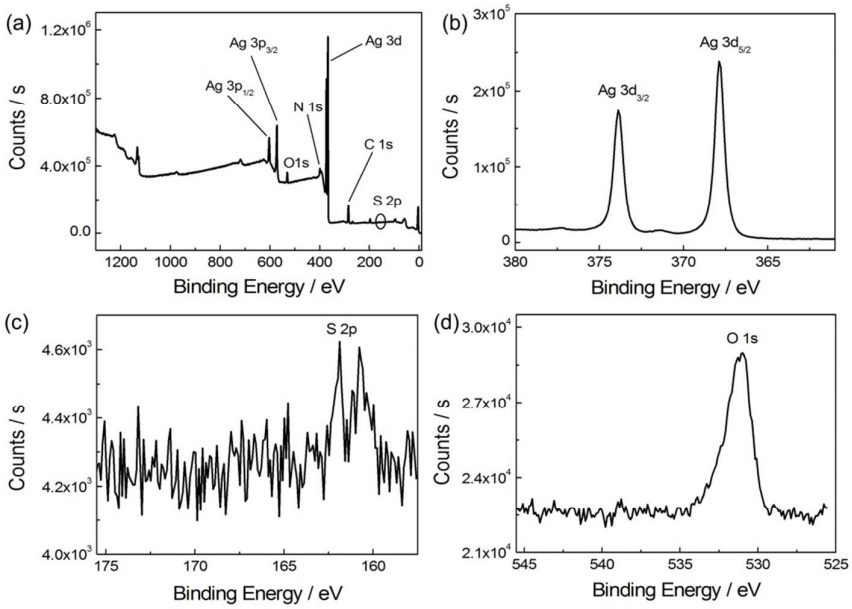


**Fig. 4** XPS characterization of Ag nanocubes that have been reacted with $K_2S_2O_8$. The XPS spectrum of all elements is shown in (a), and the spectra of Ag, S, and O are given in (b), (c), and (d), respectively.

the particles in the selected region was disappeared. Generally, the LSPR wavelength of a metal NP will blue shift when it changes from an anisotropic shape into an isotropic sphere along with the decrease of particle size.[13] However, the scattering light of an AgNC shifted to a longer wavelength before it disappeared in our work. These *illogical* phenomena might be attributed to the change of the surface status of AgNCs at the initial stage of the etching process.

In order to clarify the surface elements, X-ray photoelectron spectroscopy (XPS) was further studied after the AgNCs had been reacted with $S_2O_8^{2-}$. As shown in Fig. 4, the strong peaks located at 367.9, 373.9, 572.1, and 603.1 eV could be assigned to Ag $3d_{5/2}$, Ag $3d_{3/2}$, Ag $3p_{3/2}$, and Ag $3p_{1/2}$, respectively. In addition to Ag 3d and 3p peaks, the signal of N 1s (399.8 eV) and C 1s (284.7 eV) were also observed in the survey spectra, indicating that polyvinyl pyrrolidone (PVP), a colloidal stabilizer, could still remain on the surfaces of the nanocubes. A weak peak assigned to S 2p (161.9 eV) was also observed, which suggested that $Ag_2S$ was formed on the surface of AgNCs after the reaction. The characteristic peak of O 1s (531.0 eV) might be from the generated $Ag_2O$ at the surface or the capping agent (PVP). The results of XPS measurement indicated that the red shift of LSPR scattering during the etching was indeed caused by the formation of $Ag_2S$ and $Ag_2O$ on the surface of AgNCs.[14] Here, we believe that the $Ag_2O$ on the surface of nanocubes was dominated since the peak of S 2p was very weak. To further confirm this deduction, hydrogen peroxide ($H_2O_2$), an oxidative etchant without S, was also used for the oxidation of AgNCs beyond $S_2O_8^{2-}$, and similar result was also observed (see Fig. S3 in Supporting Information). It could be concluded that the phenomenon of red shift of LSPR scattering before it disappeared was mainly attributed to the formation of an oxide layer on the surface of AgNCs at the initial stage of the etching process.

In order to quantify the scattering light of AgNPs during the oxidative etching, we analyzed light intensity and RGB proportion of the typical three AgNPs. As shown in Fig. 5, the light intensity of particles 1-3 gradually decreased to lower than 10% of their original ones. On the other hand, the change of their RGB proportion was identical with the color changes that observed by imaging. With the increase of etching time, PB gradually decreased from ~60% to ~5%, while PG gradually increased from ~40% to ~90%. PR was always maintained at 5-10% during the whole etching process. Similar results were also obtained when $S_2O_8^{2-}$ was replaced by $H_2O_2$ as the etchant (see Fig. S4 in Supporting Information).

According to the Mie theory,[15] the scattering cross-section ($C_{sca}$) is usually used to represent the scatering ability of a metal nanoparticle,

$$C_{sca} = \frac{2\pi R^2}{x^2} \sum_{n=1}^{\infty} (2n+1)\left(a_n^{\,2} + b_n^{\,2}\right)$$

in which $R$ is the radius of the metal nanoparticle, $x$ is a particle size-related parameter, $a_n$ and $b_n$ are dependent on the following two equitions:

$$a_n = \frac{[(D_n(mx)/m + n/x)]\psi_n(x) - \psi_{n-1}(x)}{[(D_n(mx)/m + n/x)]\xi_n(x) - \xi_{n-1}(x)}$$
$$b_n = \frac{[m(D_n(mx) + n/x)]\psi_n(x) - \psi_{n-1}(x)}{[m(D_n(mx) + n/x)]\xi_n(x) - \xi_{n-1}(x)}$$

Here, $\psi_n$ and $\xi_n$ are the Riccati-Bessel functions, while $m$ is the nanoparticle-related refractive index. Therefore, the scattering property of a metal nanoparticle is relative to its physicochemical properties, the wavelength of excitation light, and the refractive index of solvent. In the present work, the wavelength of excitation light and the refractive index of solvent are constant, indicating that the scattering intensity change of the AgNPs is mainly attributed to the change of their physicochemical properties (*e.g.*, size and shape) during the etching process.

Based on this deduction, we further carefully examined the morphology change of the same AgNPs before and after they had undergone the oxidative etching. As shown in Fig. 6a, the cubic AgNPs were changed to quasi-spherical shape when they contacted with the etchant for a period of time. This remarkable morphology change demonstrated that the sharp corners of an AgNC were the preferential and primary sites involved in the oxidative etching. Thereafter, these locations would act as the most active sites for the continued etching. Once the AgNPs evolved into quasi-spherical shape, the anisotropic shape-dependent etching selectivity was disappeared. Then, the whole surface of the particles was suffered to the oxidative etching equally. Thus, the shape of the particles did not change any more but just decreased in size. More SEM images showing the morphology change of the AgNPs could be found in Supporting Information (Fig. S5).

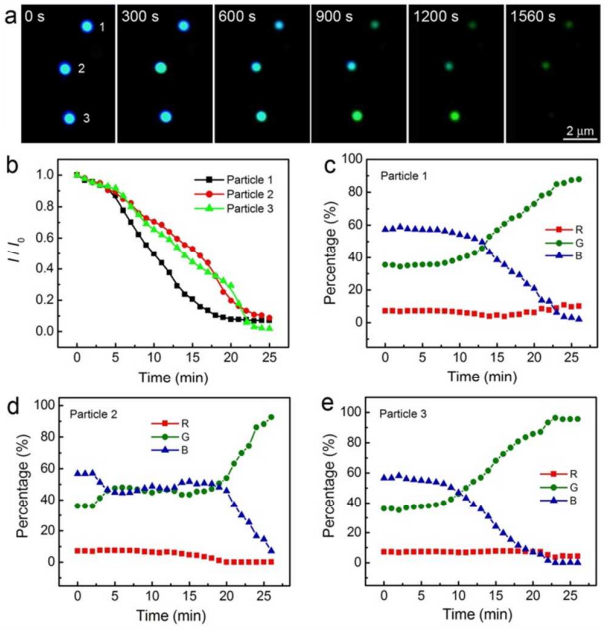


**Fig. 5** Real-time monitoring of the in situ oxidative etching of individual AgNCs by the light-scattering dark-field microscopy: (a) time-dependent images of typical three particles; (b) time-dependent intensity analysis of the corresponding particles in (a); (c-e) time-dependent RGB analysis of the corresponding particles in (a).

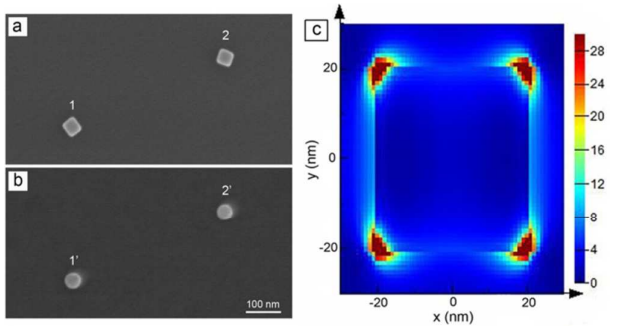


**Fig. 6** Morphology of the individual AgNPs (a) before and (b) after the oxidative etching, and (c) electromagnetic field amplitude pattern of an AgNC with edge length of 45 nm obtained by the FDTD simulation. The scattered electric field $|E|^2/|E_0|^2$ distribution results were calculated at 300-600 nm wavelength range using a 3D-FDTD method. The medium was assumed to have a constant refractive index ($n$ = 1.33). The total-field scattered-field (TFSF) light source was used with propagation normal to the image plane and E-field oscillation along the horizontal x-y plane.

In order to confirm the proposed mechanism for the oxidative etching of AgNCs, we examined the distribution of electromagnetic (EM) field strength surrounding a 45 nm AgNC (with the medium of water) using the three-dimensional finite-difference time-domain (3D-FDTD) simulation. Specifically, the incident light with the wavelength of 300-600 nm was polarized along the z axis and parallel to the underlying x-y plane of the AgNC. As shown in Fig. 6b, the region of the strongest EM field strength is located at the sharp vertices (hot-spot), then the edges and progresses toward the inside. This result verified that the continuous truncation of the AgNC leads to its transformation from a cubic shape into a sphere.

In summary, we have demonstrated that real-time monitoring of the oxidative etching on single AgNC can be achieved with the aid of an ordinary optical microscope. Combined with the optical and morphology information of the AgNPs at different stages as well as the theoretical simulation, the mechanism involved in the oxidative etching of AgNCs was clearly elucidated. Our results indicated that the oxidative etching of the AgNCs was a thermodynamics-dependent process, which started from the corners of the nanocube due to the relatively high energy at these sites. As a result, the cubic AgNPs evolved into isotropic spheres along with the decrease of particle size. We believe the proposed strategy in this work, real-time monitoring of the oxidative etching on single AgNC through optical imaging, will enable us better understand the behaviors of metal nanoparticles in a variety of chemical reactions and biological processes.

This work was supported by the National Natural Science Foundation of China (NSFC, 21035005) and startup funds from Chongqing Normal University (No. 14XLB007).

## Notes and references

1 (a) R. Jin, Y. Cao, C. A. Mirkin, K. L. Kelly, G. C. Schatz and J. G. Zheng, *Science*, 2001, **294**, 1901; (b) Y. Sun and Y. Xia, *Science*, 2002, **298**, 2176; (c) C. Burda, X. Chen, R. Narayanan and M. A. El-Sayed, *Chem. Rev.*, 2005, **105**, 1025; (d) X. Liu, D. Wang and Y. Li, *Nano Taday*, 2012, **7**, 448; (e) R. He, Y.-C.

Wang, X. Wang, Z. Wang, G. Liu, W. Zhou, L. Wen, Q. Li, X. Wang, X. Chen, J. Zeng and J. G. Hou, *Nat. Commun.*, 2014, **5**, 4327; (f) J. Sun, Y. Xianyu and X. Jiang, *Chem. Soc. Rev.*, 2014, **43**, 6239.

2 (a) G. Renaud, R. Lazzari, C. Revenant, A. Barbier, M. Noblet, O. Ulrich, F. Leroy, J. Jupille, Y. Borensztein, C. R. Henry, J.-P. Deville, F. Scheurer, J. Mane-Mane and O. Fruchart, *Science,* 2003, **300**, 1416; (b) B. Abécassis, F. Testard, O. Spalla and P. Barboux, *Nano Lett.,* 2007, **7**, 1723; (c) J. Polte, R. Erler, A. F. Thünemann, S. Sokolov, T. T. Ahner, K. Rademann, F. Emmerling and R. Kraehnert, *ACS Nano,* 2010, **4**, 1076; (d) M. Takesue, T. Tomura, M. Yamada, K. Hata, S. Kuwamoto and T. Yonezawa, *J. Am. Chem. Soc.,* 2011, **133**, 14164; (e) C. Lu, A. J. Akey, C. J. Dahlman, D. Zhang and I. P. Herman, *J. Am. Chem. Soc.,* 2012, **134**, 18732.

3 (a) C. Novo, A. M. Funston and P. Mulvaney, *Nat. Nanotechnol.,* 2008, **3**, 598; (b) T. Xie, C. Jing, W. Ma, Z. Ding, A. J. Grossc and Y.-T. Long, *Nanoscale,* 2015, **7**, 511.

4 S. Peng, J. S. Okasinski, J. D. Almer, Y. Ren, L. Wang, W. Yang and Y. Sun, *J. Phys. Chem. C,* 2012, **116**, 11842.

5 (a) Z. Wei and F. P. Zamborini, *Langmuir,* 2004, **20**, 11301; (b) G. V. Ramesh, B. Sreedhar and T. P. Radhakrishnan, *Phys. Chem. Chem. Phys.,* 2009, **11**, 10059; (c) Z. Wei, H. Qi, M. Li, B. Tang, Z. Zhang, R. Han, J. Wang and Y. Zhao, *Small,* 2012, **8**, 1331.

6 (a) H. Zheng, R. K. Smith, Y.-w. Jun, C. Kisielowski, U. Dahmen and A. P. Alivisatos, *Science,* 2009, **324**, 1309; (b) J. E. Evans, K. L. Jungjohann, N. D. Browning and I. Arslan, *Nano Lett.,* 2011, **11**, 2809; (c) H.-G. Liao, L. Cui, S. Whitelam and H. Zheng, *Science*, 2012, **336**, 1011; (d) J. M. Yuk, J. Park, P. Ercius, K. Kim, D. J. Hellebusch, M. F. Crommie, J. Y. Lee, A. Zettl and A. P. Alivisatos, *Science,* 2012, **336**, 61; (e) Y. Liu, X.-M. Lin, Y. Sun and T. Rajh, *J. Am. Chem. Soc.,* 2013, **135**, 3764; (f) Y. Jiang, G. Zhu, F. Lin, H. Zhang, C. Jin, J. Yuan, D. Yang and Z. Zhang, *Nano Lett.,* 2014, **14**, 3761.

7 (a) Y. Xiong, B. Wiley, J. Chen, Z.-Y. Li, Y. Yin and Y. Xia, *Angew. Chem. Int. Ed.,* 2005, **44**, 7913; (b) Y. Xiong, J. Chen, B. Wiley and Y. Xia, *J. Am. Chem. Soc.,* 2005, **127**, 7332; (c) C. M. Cobley, M. Rycenga, F. Zhou, Z.-Y. Li and Y. Xia, *J. Phys. Chem. C,* 2009, **113**, 16975; (d) M. J. Mulvihill, X. Y. Ling, J. Henzie and P. Yang, *J. Am. Chem. Soc.,* 2010, **132**, 268.

8 Y. Zheng, J. Zeng, A. Ruditskiy, M. Liu and Y. Xia, *Chem. Mater.,* 2014, **26**, 22.

9 (a) J. Yguerabide and E. E. Yguerabide, *Anal. Biochem.,* 1998, **262**, 137; (b) L. Q. Chen, S. J. Xiao, L. Peng, T. Wu, J. Ling, Y. F. Li and C. Z. Huang, *J. Phys. Chem. B*, 2010, **114**, 3655; (c) Y. Li, C. Jing, L. Zhang and Y.-T. Long, *Chem. Soc. Rev.,* 2012, **41**, 632; (d) Y. Liu and C. Z. Huang, *ACS Nano,* 2013, **7**, 11026; (e) B. Xiong, R. Zhou, J. Hao, Y. Jia, Y. He and E. S. Yeung, *Nat. Commun.,* 2013, **4**, 1708; (f) Y. Liu and C. Z. Huang, *Nanoscale*, 2013, **5**, 7458; (g) Y. Peng, B. Xiong, L. Peng, H. Li, Y. He and E. S. Yeung, *Anal. Chem.*, 2015, **87**, 200.

10 J. N. Anker, W. P. Hall, O. Lyandres, N. C. Shah, J. Zhao and R. P. Van Duyne, *Nat. Mater.,* 2008, **7**, 442.

11 (a) Y. Wang, Y. Zheng, C. Z. Huang and Y. Xia, *J. Am. Chem. Soc.,* 2013, **135**, 1941; (b) X. Xia, J. Zeng, L. K. Oetjen, Q. Li and Y. Xia, *J. Am. Chem. Soc.,* 2012, **134**, 1793.

12 Y. Liu, J. Ling and C. Z. Huang, *Chem. Commun.,* 2011, **47**, 8121.

13 W. Cao, T. Huang, X.-H. N. Xu and H. E. Elsayed-Ali, *J. Appl. Phys.*, 2011, **109**, 034310.

14 G. H. Chan, J. Zhao, G. C. Schatz and R. P. Van Duyne, *J. Phys. Chem. C*, 2008, **112**, 13958.

15 (a) G. Mie, *Ann. Phys.,* 1908, **25**, 377; (b) J. Ling, Y. F. Li and C. Z. Huang, *Anal. Chem.,* 2009, **81**, 1707.